1-1-2016

Expeditious and eco-friendly hydrothermal polymerization of PEDOT nanoparticles for binderfree high performance supercapacitor electrodes

Murugesan Rajesh
Dongguk University

C Justin Raj
Dongguk University

Byung Chul Kim
University of Wollongong, Dongguk University, bkim@uow.edu.au

Ramu Manikandan
Dongguk University

Sung Jin Kim
Gangneung-Wonju National University

See next page for additional authors

Expeditious and eco-friendly hydrothermal polymerization of PEDOT nanoparticles for binderfree high performance supercapacitor electrodes

Abstract

Poly(3,4-ethylenedioxythiophene) (PEDOT) is a promising conjugated polymer that has attracted attention because of its outstanding electronic properties, useful for a wide range of applications in energy storage devices. However, synthesis of high-quality PEDOT occurs via vapour phase polymerization and chemical vapour deposition techniques using extrinsic hard templates or complicated experimental setups. This study introduces a simple hydrothermal polymerization technique using ferric chloride (FeCl3) as an oxidizing agent to overcome the above drawback, which results in good conductive, crystalline PEDOT nanodendrites and nanospheres. The effects of varying the molar ratio of FeCl3 oxidant were investigated in terms of the structural, morphological and electrochemical properties of PEDOT. The supercapacitive performance of the as-polymerized PEDOT nanostructures was determined by fabricating an electrode without the aid of organic binders or conductive additives. PEDOT nanodendrites polymerized using 2.5 molar ratio of FeCl3 demonstrated enhanced electrochemical performance with a maximum specific capacitance of 284 F g-1 with high energy density of 39.44 W h kg-1 at 1 A g-1 current density in 1 M H2SO4 electrolyte. Moreover, the sample possessed higher conductivity, better specific surface area, improved electrochemical properties, comparable crystallinity, and excellent cycling stability after 5000 charge/discharge cycles than the other PEDOT nanostructures. Importantly, the results establish that these materials afford good redox behaviors with better conductivity suitable for the development of an organic electrode-based supercapacitor with high specific charge capacity and stability.

Keywords

high, performance, expeditious, eco-friendly, supercapacitor, hydrothermal, electrodes, polymerization, pedot, nanoparticles, binderfree

Disciplines

Engineering | Physical Sciences and Mathematics

Publication Details

Rajesh, M., Raj, C. Justin., Kim, B. Chul., Manikandan, R., Kim, S., Park, S. Yeup., Lee, K. & Yu, K. Hyun. (2016). Expeditious and eco-friendly hydrothermal polymerization of PEDOT nanoparticles for binderfree high performance supercapacitor electrodes. RSC Advances: an international journal to further the chemical sciences, 6 (111), 110433-1-110443-11.

Authors

Murugesan Rajesh, C Justin Raj, Byung Chul Kim, Ramu Manikandan, Sung Jin Kim, Sang-Yeup Prof Sang-Yeup Park, Kwangsoo Lee, and Kook Hyun Yu

RSC Advances

PAPER

View Article Online
View Journal | View Issue

Cite this: *RSC Adv.*, 2016, **6**, 110433

Expeditious and eco-friendly hydrothermal polymerization of PEDOT nanoparticles for binder-free high performance supercapacitor electrodes†

Murugesan Rajesh,[a] C. Justin Raj,*[a] Byung Chul Kim,[ab] Ramu Manikandan,[a] Sung-Jin Kim,[c] Sang Yeup Park,[c] Kwangsoo Lee[d] and Kook Hyun Yu*[a]

Poly(3,4-ethylenedioxythiophene) (PEDOT) is a promising conjugated polymer that has attracted attention because of its outstanding electronic properties, useful for a wide range of applications in energy storage devices. However, synthesis of high-quality PEDOT occurs *via* vapour phase polymerization and chemical vapour deposition techniques using extrinsic hard templates or complicated experimental setups. This study introduces a simple hydrothermal polymerization technique using ferric chloride ($FeCl_3$) as an oxidizing agent to overcome the above drawback, which results in good conductive, crystalline PEDOT nanodendrites and nanospheres. The effects of varying the molar ratio of $FeCl_3$ oxidant were investigated in terms of the structural, morphological and electrochemical properties of PEDOT. The supercapacitive performance of the as-polymerized PEDOT nanostructures was determined by fabricating an electrode without the aid of organic binders or conductive additives. PEDOT nanodendrites polymerized using 2.5 molar ratio of $FeCl_3$ demonstrated enhanced electrochemical performance with a maximum specific capacitance of 284 F g^{-1} with high energy density of 39.44 W h kg^{-1} at 1 A g^{-1} current density in 1 M H_2SO_4 electrolyte. Moreover, the sample possessed higher conductivity, better specific surface area, improved electrochemical properties, comparable crystallinity, and excellent cycling stability after 5000 charge/discharge cycles than the other PEDOT nanostructures. Importantly, the results establish that these materials afford good redox behaviors with better conductivity suitable for the development of an organic electrode-based supercapacitor with high specific charge capacity and stability.

Received 14th September 2016
Accepted 28th October 2016

DOI: 10.1039/c6ra22958a

www.rsc.org/advances

1. Introduction

Growing demands for high energy storage systems have driven research efforts towards development of sustainable and renewable energy sources. Supercapacitors are electrochemical energy storage devices that can provide relatively high power and comparable energy densities based on the charge storage occurrence of faradic redox reactions or electrical double layer formation in the electrodes. Generally, supercapacitor electrodes are fabricated using either pseudocapacitance materials such as transition metal oxides or electrically conducting polymers (ECPs), or electrical double layer capacitance materials such as carbonaceous material with high surface area.[1] In recent years, ECPs nanostructures (*e.g.*, polyaniline (PANI), polypyrrole (PPy) and poly(3,4-ethyelenedioxythiophene) (PEDOT)) have received greater interest than carbon materials or transition metal oxides because of their high conductivity, chemical stability, low cost, high doping–dedoping capability, easy synthesis, *etc.*[2] PEDOT is a thermally stable, highly conductive, conjugated polymer, with potential applications in photovoltaics, light emitting diodes, sensors, actuators and thin film transistors.[3] Synthesis of micro or nanostructured PEDOT can be focused to improve its remarkable physical and chemical properties for various applications. The advantages of using polymer nanostructures as advanced electrochemical electrodes are large active surface area, high electric, thermal conductivity and excellent connection between active materials and substrates. These properties facilitate high electron transfer rate, prevent agglomeration and improve penetration of electrolytes into the active site of the polymer matrix for excellent charge storage in supercapacitor electrodes. There are some reliable methods for fabrication of PEDOT nanostructures using template-assisted synthesis, such as surfactant micelles,[4–7] mesoporous and microsphere silica,[8–10] reverse micro emulsion

[a]*Department of Chemistry, Dongguk University-Seoul, Jung-gu, Seoul-100715, South Korea. E-mail: yukook@dongguk.edu; cjustinraj@gmail.com; Tel: +82 2 2260 3709*
[b]*ARC Centre of Excellence for Electromaterials Science, IPRI, AIIM Facility, University of Wollongong, Innovation Campus, NSW 2522, Australia*
[c]*Department of Ceramic Engineering, Gangneung-Wonju National University, Gangneung-210-702, Republic of Korea*
[d]*Photo-Electronic Hybrids Research Center, Korea Institute of Science and Technology, Seoul-02-792, Republic of Korea*

† Electronic supplementary information (ESI) available: Additional figures and tables related to this article. See DOI: 10.1039/c6ra22958a

polymerization,[11] reverse interfacial polymerization,[12] self-assembly membrane synthesis[13] and electrochemical polymerization in the presence of aluminium oxide template and surfactant.[14,15] However, it is difficult to obtain highly conducting PEDOT nanostructures *via* template-free, simple solution-based techniques.

Generally, PEDOT acquires the highest conductivity when synthesized *via* a vapour phase solution method.[16,17] Controllable nanostructures of PEDOT had been polymerized using high temperature vapour phase synthesis approaches such as physical vapour deposition or chemical vapour deposition and also solution-based chemical strategies including electrochemical synthesis and sol gel technique.[18,19] Moreover, highly conducting PEDOT surface layers have been achieved by oxidative chemical vapour phase polymerization,[20–22] evaporative vapour phase polymerization,[23] and ultrasonic spray polymerization methods.[24]

The electrical conductivity of ECPs arises from charge carriers induced by chemical doping and the mobility of the charge carriers along conjugated polymer matrix chains.[25] The energy storage mechanism of ECP electrodes depends mainly on the electrochemical performance in terms of specific capacitance, rate capability and cycling stability. These factors depend on their surface morphology, crystallinity and degree of polymerization, which originates from the synthesis process. Zhang *et al.* synthesized PEDOT microspheres by an ultrasonic spray polymerization method using $FeCl_3$ as oxidant, which exhibited a maximum specific capacitance value of 150 F g^{-1}.[24] Zhao *et al.* synthesized coral-like morphology of PEDOT by a chemical oxidation method using $FeCl_3$, which showed a specific capacitance of 174 F g^{-1}.[26] Sohn *et al.* reported PEDOT nanorods decorated on graphene foam by a chemical deposition method using $FeCl_3$, which demonstrate a specific capacitance value of 97 F g^{-1}.[27] However, use of toxic reagents, harsh synthetic processes and demand for expensive instruments has limited their potential in commercial applications. Therefore, methods for facile and environmentally friendly large-scale synthesis of PEDOT nanostructures would be significant, and improvement of the electrochemical properties of such nanostructure is in great demand for supercapacitor applications. Comparing the above mentioned methods, hydrothermal synthesis offers an alternative technique for high temperature solution-based chemical strategies, as this is considered to be a more affordable synthesis technique for nanostructured materials on a large scale. Vapour phase polymerization methods are expensive and energy-consuming in comparison with hydrothermal synthesis. In hydrothermal conditions the chemical reactions are performed inside a sealed container above ambient temperature and pressure to grow the appropriated nanostructures.[28] Moreover, hydrothermal synthesis can produce controlled nanostructures of varying morphology more safely and economically, with resultant high-quality nanostructures.

Herein, we report, for the first time, a method for simple, template-free and eco-friendly hydrothermal synthesis to polymerize highly conducting and crystalline PEDOT nanostructures using varying molar ratios (MR) of oxidant $FeCl_3$ (ferric chloride hexahydrate). These PEDOT nanostructures exhibited excellent electrochemical performance in the form of binder-free supercapacitor electrodes and showed high specific capacitance value of 284 F g^{-1}, which is higher than previously reported values. Moreover, the effect of varying molar ratios of oxidizing agent was studied on structural, morphological and supercapacitive properties of PEDOT nanostructure under hydrothermal polymerization, and results are discussed in detail.

2. Experimental section

2.1 Materials

The 3,4-ethylenedioxythiophene (EDOT) (purity >98%) was purchased from Tokyo Chemicals Industry Co Ltd., Japan, ferric chloride hexahydrate ($FeCl_3 \cdot 6H_2O$) extra pure (assay-98%) was obtained from Daejung chemicals (Korea), graphite rods were purchased from Sigma-Aldrich (Korea), and sulphuric acid (95%) and ethanol were purchased from Samchun Pure Chemicals Co Ltd., Korea. All reagents were analytical grade and used without further purification.

2.2 Hydrothermal polymerization of PEDOT and supercapacitor electrode fabrication

The hydrothermal polymerization was performed by mixing 25 ml (0.7109 g) of 0.2 M solution of 3,4-ethylenedioxythiophene (EDOT) with 25 ml (3.38 g) of 2.5 molar ratio (MR) of ferric chloride hexahydrate solution prepared in 50 : 50 ethanol/water mixture. The resultant mixture was stirred for 30 minutes at room temperature and transferred to a 100 ml capacity teflon-lined stainless steel autoclave for hydrothermal reaction at 150 °C for 15 h. This cationic radical polymerization yielded a conjugated PEDOT backbone chain with a dark blue coloured precipitate.[29,30] The reaction mixture was then allowed to cool to room temperature and the dark blue precipitate was collected through filtration and washed repeatedly using aqueous alcoholic (50 : 50) solution. Finally, the product was dried at 90 °C for 12 h. The above synthesis method was adopted for preparation of other MR of (1.25, 3.75 and 5) $FeCl_3$ oxidant-based PEDOT nanostructures. The resultant hydrothermally synthesized PEDOT samples were denoted as 1.25 MR $FeCl_3$, 2.5 MR $FeCl_3$, 3.75 MR $FeCl_3$ and 5 MR $FeCl_3$, respectively. Fig. 1 is a schematic representation of the polymerization reaction and shows formation of various morphological nanostructures with respect to the different molar ratios of $FeCl_3$.

The supercapacitor electrodes were fabricated by dispersing the synthesized PEDOT nanostructures in ethanol solution without addition of any binder or supporting conductive materials to form slurry. The slurry was then pasted onto a polished graphite surface, which acts as a current collector (as shown in Fig. S1†), and dried at 85 °C for 12 h in a vacuum oven. The mass of active PEDOT samples coated on the graphite rod is ~1.5 mg.

2.3 Characterization and electrochemical measurements

The PEDOT electrode materials were characterized using SEM, TEM, XRD, Raman, FTIR, UV and EDX measurements.

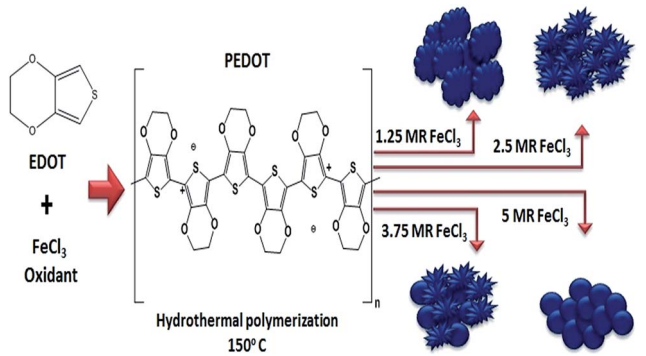

Fig. 1 Formation of various PEDOT nanostructures by hydrothermal polymerization.

Microstructural features and elemental analysis (EDX) of PEDOT nanostructures were recorded using a field emission scanning electron microscope (FESEM) (JEOL-7500FA field emission SEM (Japan)) and transmission electron microscope (TEM) (JEOL (Japan) model JEM-2100F), respectively. Raman spectra were recorded using a Micro Raman spectrometer with excitation produced by a laser beam at 525 nm wavelength. The crystallinity and structure of PEDOT materials were analyzed by X-ray diffraction (XRD, D/max-2400, Rigaku, Ultima IV) using a Cu Kα source operated at 40 kV and 30 mA in the 2θ range of 0–80°. The FTIR spectra of the polymer nanostructures were obtained using a Fourier transform infrared spectrometer (Thermo Electron Nicolet 6700, frequency range 500–4000 cm^{-1}). The UV-visible spectra of the samples were recorded using a Varian cary-50 UV-vis spectrophotometer. The conductivity of the samples were measured by a two-probe technique using Keithley 2100 digit multimeter at room temperature. For conductivity measurements, the samples were pressed into a pellet of diameter 130 mm and thickness ~0.81 mm. Both sides of the pellet were coated with a silver paste, which acts as a parallel electrode. The sheet resistance of the electrodes was tested using the Keithley 2100. The Brunauer–Emmett–Teller (BET) specific surface area of the samples was measured using a Quantachrome NOVA 2200e instrument (USA). The supercapacitive performance of the PEDOT nanostructures electrodes was tested at room temperature using a ZIVE-SP2 LAB (South Korea) electrochemical workstation with a three-electrode configuration, having Pt wire as the counter electrode, Ag/AgCl as the reference electrode, and the PEDOT polymer nanostructures coated on graphite as the working electrode in 1 M H_2SO_4 electrolyte. Cyclic voltammetry (CV) was performed for various scan rates from 5 to 300 mV s^{-1} and a galvanostatic charge/discharge (GCD) test was carried out for various charge/discharge current densities 1, 2.5, 5, 7.5, 10, 12.5, 15, 17.5 and 20 A g^{-1} within a potential range of −0.2 to 0.8 V. Electrochemical impedance spectroscopy (EIS) was investigated in the frequency range of 10 mHz to 100 kHz at 0 V bias condition. Cycling stability measurements for different nanostructured PEDOT electrodes were recorded by performing sequential GCD tests at a constant 10 A g^{-1} current density for 5000 cycles.

2.4 Calculation of specific capacitance, energy and power density

The specific capacitance (C) value of the electrodes was calculated from CV data according to eqn (1)

$$C = \frac{\int i\mathrm{d}v}{2 \times m \times s \times \Delta V} \quad (1)$$

where $\int i\mathrm{d}v$ is the total integral area of the charge and discharge curve, m is the mass of electroactive material coated on the electrode, s is scan rate (mV s^{-1}) and ΔV is the applied potential window of the CV curve.

Specific capacitance (C_s) values from galvanostatic charge/discharge curves were calculated by eqn (2),

$$C_s = \frac{I \times \Delta t}{\Delta V \times m} \quad (2)$$

where I is the applied current (A), Δt is the discharge time, ΔV is the applied potential window of the GCD curve and m is the mass of active material in the electrode.

The energy density (E) and power density (P) of the electrodes were estimated according to,

$$E = \frac{1}{2} C \Delta V^2 \quad (3)$$

and

$$P = \frac{E}{\Delta t} \quad (4)$$

where E is the energy density (W h kg^{-1}), P is the power density (W kg^{-1}), C is the specific capacitance of the electrodes, Δt is the discharge time and ΔV is the operating potential window (V).

3. Results and discussion

3.1 Morphological analysis

The surface morphologies of PEDOT nanostructures synthesized *via* varying concentrations of oxidant ($FeCl_3$), were recorded by scanning electron microscopy (SEM) and the resultant images are shown in Fig. 2(a–d). Significantly slight changes in PEDOT morphologies were observed while increasing the MR of $FeCl_3$. All the samples show irregular morphology as is generally observed for polymeric materials. In the case of 1.25 and 2.5 MR of $FeCl_3$, polymerized PEDOT nanoparticles show almost blending of grains like polymer growth. The PEDOT nanoparticles obtained from 3.75 MR of $FeCl_3$ show a mixed form of small grain size growth with highly aggregated spherical nanostructures. The sample from 5 MR of $FeCl_3$ shows a highly agglomerated form of nanostructure. Generally, the morphology of PEDOT displays a regular variation with increasing molar ratio of oxidant, with increasing oxidant redox potential affording formation of different PEDOT nanostructures.[31] However, the obtained SEM images do not allow determination of the exact morphology of the samples because of formation of small polymeric nanoparticles. So, to attain clear structural information the resultant samples were subjected to TEM analysis.

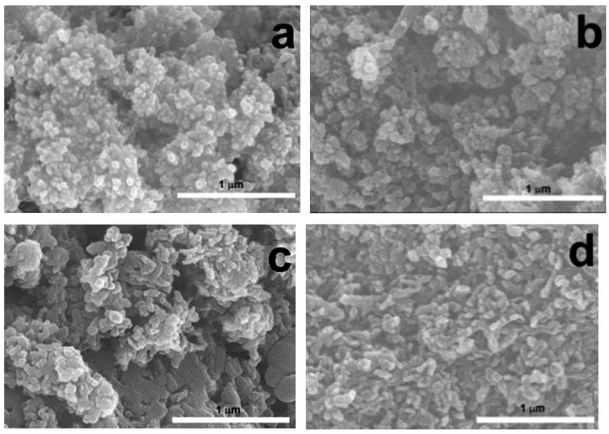

Fig. 2 SEM images of PEDOT nanoparticles obtained from the oxidant (a) 1.25 MR of $FeCl_3$; (b) 2.5 MR of $FeCl_3$; (c) 3.75 MR of $FeCl_3$ and (d) 5 MR of $FeCl_3$.

Fig. 3(a–d) shows the obtained transmission electron microscopy (TEM) images of the PEDOT nanostructures prepared using varying MR of $FeCl_3$. From the image, 1.25 and 2.5 MR of $FeCl_3$ polymerized PEDOT samples show a bunch of comparatively small-sized PEDOT nanoparticles with dendrite growth in the polymer. Increasing the $FeCl_3$ concentration to 5 MR caused the nanodendrite structure growth to completely transfer to large-sized spherical morphology. But the 3.75 MR of $FeCl_3$ sample shows a mixed form of spherical and highly aggregated nanodendrites with slightly larger sized particles. At low concentration of oxidant the polymerization process is slow and tends to form tiny nanodendrite oligomers, which may act as a soft template for growth of nanodendrites such as PEDOT. But at high MR of $FeCl_3$, the rate of PEDOT polymerization is very aggressive and restricts the growth of soft template nanodendrites because of the powerful charge of oxidant concentrations and leads to formation of large aggregated nanospheres.[32] Fig. 3 shows that the nanodendrite growth is denser for 2.5 MR of $FeCl_3$ polymerized sample compared with 1.25 MR of $FeCl_3$ sample because optimum or sufficient amount of oxidants are involved in the polymerization. Above this optimum level of $FeCl_3$, the PEDOT nanodendrites start to agglomerate and tend to form large-sized agglomerated nanospheres. Fig. 4a–d shows high resolution TEM images of the PEDOT nanostructures synthesised using varying MR of $FeCl_3$. It can clearly be seen that the 2.5 MR $FeCl_3$ sample exhibits polymer growth as extended disordered dendritic growth in the ending face similar to the vapour phase polymerization method, which reveals the anisotropic crystal formation of the sample.[16] In the case of higher MR of $FeCl_3$ the dendritic type of polymer growth was restricted in the ending face, and resembles spherical growth. Thus the nanodendrite structures entwine with each other and construct plenty of diminutive pores in each cluster of dendrites, which effectively promote the possibility of large ion storage and ion transport.[7] These results depict that by controlling the MR of oxidants in hydrothermal conditions, efficient morphological PEDOT nanostructures can be achieved for energy storage applications.

3.2 Structure studies

3.2.1 X-ray diffraction. Fig. 5(a) shows the XRD patterns of PEDOT nanoparticles synthesized *via* hydrothermal polymerization using various MR of $FeCl_3$. The resultant XRD have a characteristic peak at $2\theta = 6.4^\circ$ corresponding to the lamella stacking distance $d_{(100)}$, which can be attributed to the average distance between the ladder-like PEDOT molecules in the plane, and a second order peak was slightly exhibited at 12.8°.[33–35] The average $d_{(100)}$ distance between the stacking of PEDOT chains mainly depends on the dopant ions used in the PEDOT polymerization process. Furthermore, all samples show a high angle reflection at $2\theta = 26^\circ$, which is indexed to be the interchain

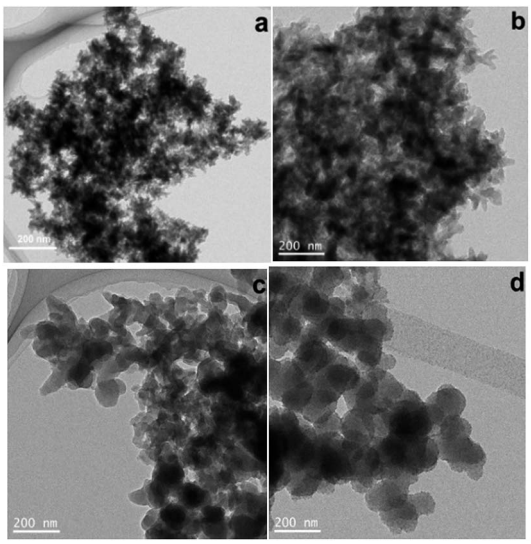

Fig. 3 TEM images of PEDOT nanoparticles prepared using (a) 1.25 MR of $FeCl_3$; (b) 2.5 MR of $FeCl_3$; (c) 3.75 MR of $FeCl_3$ and (d) 5 MR of $FeCl_3$.

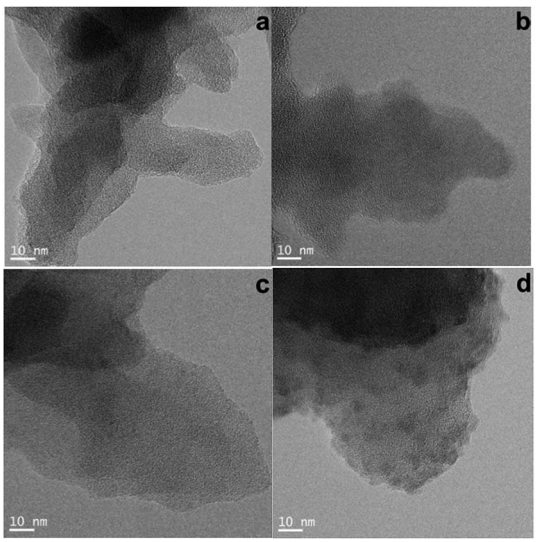

Fig. 4 HRTEM images of PEDOT nanoparticles obtained from (a) 1.25 MR of $FeCl_3$; (b) 2.5 MR of $FeCl_3$; (c) 3.75 MR of $FeCl_3$ and (d) 5 MR of $FeCl_3$.

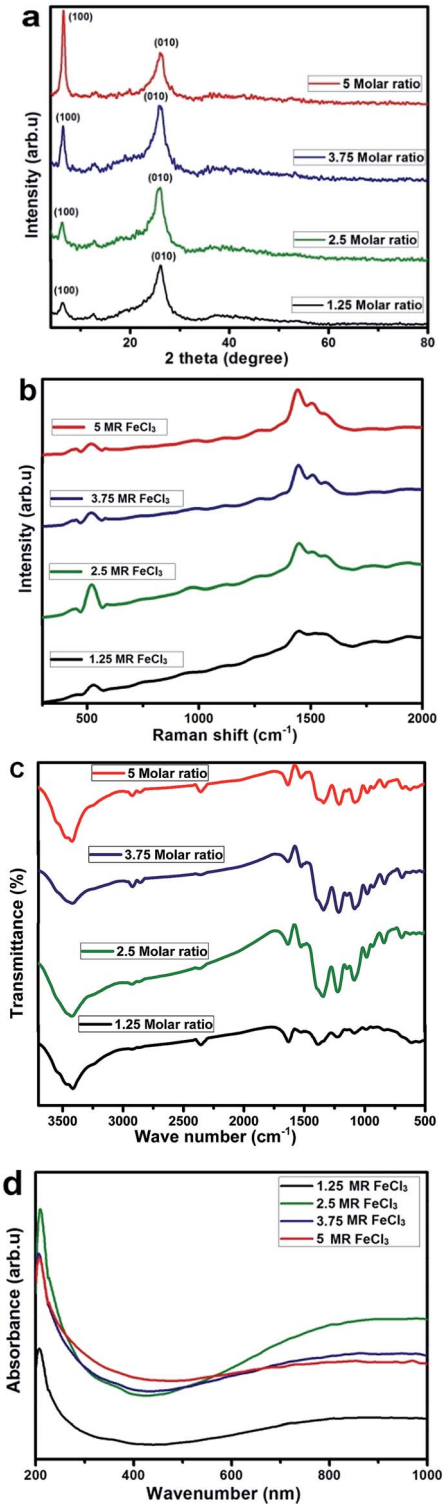

Fig. 5 (a) XRD patterns, (b) Raman spectra, (c) FTIR spectra and (d) UV-visible spectra of the PEDOT samples synthesized from various MR of $FeCl_3$.

planar π–π stacking distance $d_{(010)}$ of the aromatic rings of PEDOT.[36] The intensity of the (100) peak ($2\theta = 6.4^\circ$) increased with respect to increasing MR of $FeCl_3$, indicating increased lamella stacking distance and improved crystallinity of the sample. At the same time, reduction in intensity of the (100) peak in low MR $FeCl_3$ samples reveals a decrease in doping level.[37,38] The anisotropic nature formation of PEDOT nanoparticles means that exist in both crystalline and amorphous forms. The crystalline portion is in the lamella and the amorphous portion is outside the lamella. The percentage of crystallinity (X_c) is calculated according to eqn (5),

$$X_c = \frac{A_c}{A_a + A_c} \times 100\ \% \quad (5)$$

where A_c is the area of crystalline phase and A_a is the area of amorphous phase.

From the calculated value, the crystallinity percentage of PEDOT nanostructures increases with respect to increase in MR of $FeCl_3$, that is 32, 36, 43 and 65% for 1.25, 2.5, 3.75 and 5 MR of $FeCl_3$, respectively. The obtained result is in good agreement with that reported for vapour phase polymerization of PEDOT, which also leads to a well-ordered crystalline structure and exhibited strong reflective intensity at $2\theta = 6.4^\circ$ for high concentration of oxidant.[16,39] The conductivity and efficiency of electrical transport properties are not solely related to the degree of crystallinity, because the amorphous forms are penetrated more by the solvents or electrolytes than their crystalline counterparts.[40] Comparing all hydrothermally polymerized PEDOT nanoparticles, the sample with 2.5 MR of $FeCl_3$ exhibited comparable crystallinity with higher intensity of amorphous form (shown in Fig. S2†). This optimum level of doping and the pronounced nanostructures with dendritic growth of 2.5 MR of $FeCl_3$ make this a potential candidate for electrochemical supercapacitor electrodes.

3.2.2 Raman spectroscopy. The Raman spectra of various MR of $FeCl_3$-based PEDOT nanoparticles are overlaid in Fig. 5(b). The Raman spectrum of PEDOT exhibits more significant strong absorption at 1445 cm^{-1}, that is the characteristic peak of symmetric $C_\alpha{=}C_\beta$ (–O), with stretching vibration and noticeable peaks at 1510 cm^{-1} and 1560 cm^{-1} representing the asymmetric stretching mode of $C_\alpha{=}C_\beta$ and indicative of a high level of oxidation in the polymer matrix. The high peak intensity of symmetric stretching $C_\alpha{=}C_\beta$ in polymer is attributed to the increase in proportion of the oxidized structures in PEDOT. The obtained spectrum displays that the peak intensity of symmetric stretching of $C_\alpha{=}C_\beta$ in polymer increases with respect to increase in the MR of $FeCl_3$, this clearly indicates that oxidation tendency was increased in the polymer with respect to higher molar ratio of oxidants.[41–43] Comparing all the spectra, large MR $FeCl_3$-based PEDOT samples exhibited a high level of conjugation in their polymer chain, in contrast to the low (1.25) MR $FeCl_3$-based PEDOT nanoparticles. The band arising from the $C_\beta{=}C_\beta$ stretching vibration was close to 1365 cm^{-1} and the inter-ring stretching of $C_\alpha{=}C_{\alpha'}$ was observed at 1267 cm^{-1}. The deformation of C–O–C bond led to a peak at around 1100 cm^{-1} and the oxyethylene ring deformation peak was at approximately 980 cm^{-1}. The peaks at 710 cm^{-1} and 580 cm^{-1} resulted from symmetric C–S–C ring deformation and oxyethylene deformation of the polymer, respectively.[22]

3.2.3 Infrared spectroscopy. The FTIR spectra of PEDOT nanoparticles prepared using different MR of $FeCl_3$ are shown in Fig. 5(c). The spectrum of PEDOT shows wide band occurring

at 3450 cm^{-1}, which is likely to be attributed to –OH stretching vibrations resulting from the hygroscopic nature of the dopant.[44,45] The peak observed at 1577 cm^{-1} is attributed to the conjugative C=C system, which determines the conductivity of the synthesized PEDOT nanostructures.[17] Similarly, the less intense peak at 1577 cm^{-1} for 1.25 MR of $FeCl_3$ polymerized PEDOT clearly indicates that low MR of $FeCl_3$ is insufficient for complete polymerization and results in poor conductivity compared with the higher MR of $FeCl_3$ samples. The bands at 1340 and 1577 cm^{-1} show the C–C and C=C stretching of the quinoid structure of the thiophene ring and the ring stretching vibration, respectively. The peaks appearing at approximately 1214, 1146 and 1083 cm^{-1} are attributed to the bending vibration of alkylenedioxy (C–O–C) groups. The peaks corresponding to 980, 833 and 682 cm^{-1} are assigned to characteristic vibrations of the C–S–C bonds in thiophene. The above FTIR analysis confirms the successful formation of the PEDOT polymeric nanostructure *via* hydrothermal polymerization.

3.2.4 UV-visible absorption spectra. Fig. 5(d) shows the UV-visible absorption spectra of hydrothermally polymerized PEDOT nanoparticles using different MR of $FeCl_3$. All the PEDOT nanoparticles showed significant absorbance change around 640–660 nm and exhibited high absorbance above the 700 nm region. These absorption changes >700 nm correspond to the density of polaronic states or conjugation length, which also influence the electrical conductivity of the PEDOT polymer chain.[46] Clearly, the 1.25 MR $FeCl_3$-based PEDOT nanoparticles exhibit very low absorbance compared with the samples with higher MR. Moreover, the 2.5 MR $FeCl_3$-polymerized PEDOT nanoparticles exhibited broad and high absorption above 700 nm compared with 3.75 and 5 MR of $FeCl_3$. This reveals the existence of high electrical conductivity and the conjugation length of 2.5 MR of $FeCl_3$-based PEDOT nanoparticles. The absorption band in the 640-660 nm region can be attributed to the π–π^* transition associated with excitation of electrons across the band gap of the delocalized conductive metallic state of PEDOT.[47]

3.2.5 Energy dispersive X-ray spectroscopy (EDX). The EDX analysis shows (Fig. S3†) the doping level of different nanostructures of PEDOT nanoparticles obtained from various MR of $FeCl_3$. From the analysis traces of chloride were observed in 1.25 MR $FeCl_3$-polymerized PEDOT nanoparticles, suggesting that the low molar ratio of oxidant is not sufficient for complete polymerization. While increasing the MR of $FeCl_3$ in the polymerization process, the atomic percentage of chloride content rises as 0.36, 0.78 and 0.99 for 2.5, 3.75 and 5 MR of $FeCl_3$, respectively (Fig. S3 and Table S1†). Furthermore determination of Fe content by EDX typically shows that the Fe content is below the limit 0.05% for 2.5 MR $FeCl_3$-based PEDOT nanoparticles, compared with 0.18 and 0.28% for 3.75 and 5 MR $FeCl_3$ samples, respectively.

3.2.6 Specific surface area analysis. The specific surface area of the PEDOT nanoparticles was obtained from adsorption and desorption analysis using the N_2 gas isotherm method. The BET surface areas of PEDOT nanoparticles were calculated to be 64.94 $m^2\ g^{-1}$, 77.97 $m^2\ g^{-1}$, 68.22 $m^2\ g^{-1}$ and 69.52 $m^2\ g^{-1}$ for 1.25, 2.5, 3.75 and 5 MR $FeCl_3$ used for the polymerization process, respectively, as shown in Fig. S4.† From this analysis, it is confirmed that the 2.5 MR $FeCl_3$-polymerized PEDOT nanoparticles have better surface area because of optimum doping level with nanodendrite growth of PEDOT nanoparticles during the polymerization process compared with lower and higher MR of $FeCl_3$ concentration. The 5 MR $FeCl_3$-polymerized PEDOT nanoparticles display almost the same surface area as 3.75 MR $FeCl_3$, indicating uniform growth of spherical nanoparticles occurring in the 5 MR $FeCl_3$ polymerization process. But the 3.75 MR $FeCl_3$ PEDOT nanoparticles show a mixed form of aggregate nanodendrites with minor spherical morphology structure. Hydrothermally synthesized PEDOT nanoparticles show higher BET surface area than that of samples synthesized *via* ultrasonic spray polymerization and micro emulsion template methods.[6,24]

3.3 Electrochemical performance

3.3.1 Cyclic voltammetry. The electrochemical properties of the electrodes were characterized using cyclic voltammetry analysis.

The resultant cyclic voltammograms of the different MR of $FeCl_3$ synthesized PEDOT electrodes at 25 mV s^{-1} scan rate in 1 M H_2SO_4 are shown in Fig. 6(a). The curves reveal that PEDOT nanoparticles polymerized using 2.5 MR of $FeCl_3$ possess better electrochemical property with enhanced background current compared with the other electrodes. All CV curves have an almost rectangular shape with a broad redox peak, except for the 1.25 MR $FeCl_3$-based PEDOT sample, which is attributed mainly to partial oxidation of the polymer chain compared with the other samples. Comparing the oxidation and reduction potentials of 1.25 MR $FeCl_3$-based PEDOT electrodes of approximately 0.1 V and 0.3 V, with those of other higher MR $FeCl_3$-based PEDOT electrodes which show very proximity redox potential values (0.3 V and 0.37 V), highlights the partial polymerization of the 1.25 MR $FeCl_3$ sample. PEDOT polymerized using 2.5 MR $FeCl_3$ with high surface area nanodendrite-like structures showed better capacitive property because of charge-balancing of anion every three EDOT monomer units.[48] Fig. 6(b) shows the variation of specific capacitance values with respect to increase in scan rate from 5 to 300 mV s^{-1} for various MR $FeCl_3$-polymerized PEDOT electrodes. From this plot, the PEDOT polymerized using 2.5 MR $FeCl_3$-based electrode exhibits high specific capacitance values at all scan rates. Moreover, the rate capability of ~42% up to 300 mV s^{-1} is also more favourable for 2.5 MR $FeCl_3$-based electrodes when compared with other MR $FeCl_3$-based electrodes. The 1.25 MR $FeCl_3$-based electrode shows only 16% rate capability with drastically diminished specific capacitance values at higher scan rates, representing the poor rate capability of the sample. All the electrodes show the same trend of decrease in capacitance values with respect to increase in scan rates. At lower scan rate the electrolyte ions have sufficient time to penetrate the whole active material and show high capacitance, whereas at higher scan rates the electrolyte ions accumulate on the outer surface only, so having reduced possibility of charge storage.[49] The 1.25 MR $FeCl_3$-based PEDOT electrode shows comparable

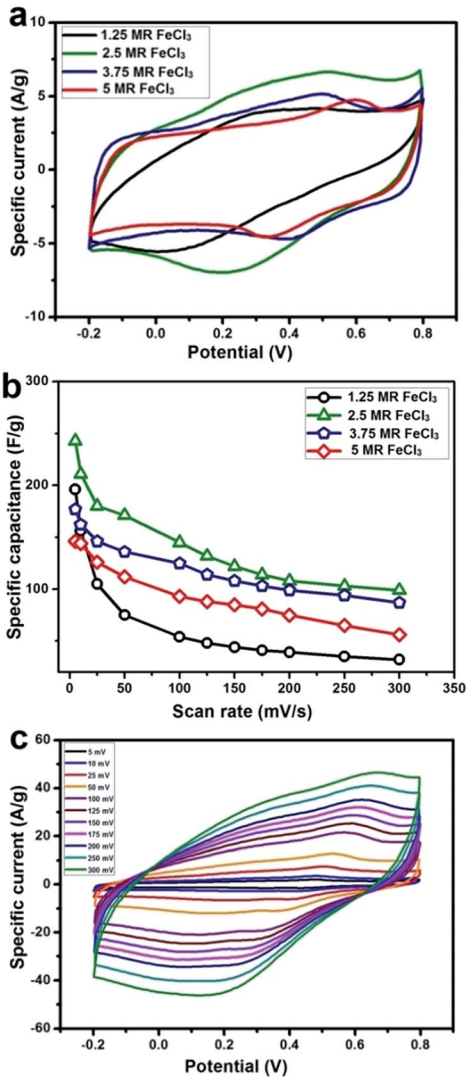

Fig. 6 (a) Cyclic voltammograms of PEDOT electrodes measured at 25 mV s^{-1} scan rate prepared from various MR of $FeCl_3$; (b) scan rate dependent specific capacitance values of PEDOT electrodes (5 to 300 mV s^{-1} scan rates) obtained from different MR of $FeCl_3$ and (c) cyclic voltammograms of 2.5 MR of $FeCl_3$ polymerized PEDOT electrodes from 5 to 300 mV s^{-1} scan rates.

specific capacitance at low scan rate with other high MR $FeCl_3$ (3.75 and 5)-based PEDOT electrodes perhaps because of the less crystalline nature of the sample and similar nanodendrite structure to that of the efficient 2.5 MR $FeCl_3$-based electrode. To further corroborate the above result, the conductivity of the samples were determined (Fig. S5†). The conductivity values calculated for 1.25, 2.5, 3.75 and 5 MR $FeCl_3$-based PEDOT samples were 1.4, 2.9, 1.1 and 0.79 mS cm^{-1}, respectively. The sheet resistances for various MR $FeCl_3$-based PEDOT electrodes (1.25, 2.5, 3.75 and 5 MR of $FeCl_3$) were 8.82, 4.26, 11.22 and 15.62 kΩ cm^2, respectively. These results suggest that an increase in MR of $FeCl_3$ corresponds to a decrease in conductivity of the samples gradually after 2.5 MR $FeCl_3$.[50] The 2.5 MR $FeCl_3$-polymerized PEDOT nanoparticles show the higher conductivity and lower sheet resistance value than the other samples.

Fig. 6(c) depicts the cyclic voltammograms of 2.5 MR $FeCl_3$-PEDOT electrodes for various scan rates ranging from 5 to 300 mV s^{-1}. The scan rate-dependent cyclic voltammograms of other MR of $FeCl_3$-polymerized PEDOT electrodes are shown in Fig. S6.† The shape of the CV curves indicates a clear reversible redox reaction (faradic reaction) because of the pseudocapacitive nature of the PEDOT nanostructures. The electrochemically reversible redox reactions are diffusion controlled processes as characterized by the linear relationship between peak current and square root of the scan rate (Fig. S7†). The figure shows that the oxidation and reduction peaks shift to more positive and negative positions with increasing scan rate because of the increment of the internal diffusion resistance in the electrode material.[51,52] The 2.5 MR $FeCl_3$-based nanodendrite structure with optimum level of doping, better surface area, more proportionate crystallinity and diffusion site shows enhanced electrochemical properties compared with the other nanostructured PEDOT electrodes.

3.3.2 Galvanostatic charge discharge. Galvanostatic charge/discharge tests were performed to evaluate the exact capacitance of different MR $FeCl_3$-polymerized PEDOT electrodes. Fig. 7(a) shows the comparative charge/discharge profiles of all the electrodes at a constant current density of 1 A g^{-1}. The galvanostatic charge/discharge curves exhibited an ideal triangular shape, indicating the process of faradic reaction during charging and discharging process.[53] The resultant experiment indicates that 2.5 MR $FeCl_3$-based PEDOT electrode exhibited a maximum specific capacitance value of 284 F g^{-1} at 1 A g^{-1} charge/discharge current density. Moreover, galvanostatic charge/discharge tests were performed for 2.5 MR $FeCl_3$ electrodes for various charge/discharge current densities 1, 2.5, 5, 7.5, 10, 12.5, 15, 17.5 and 20 A g^{-1}, as shown in Fig. 7(b). The electrode shows charge/discharge time decreases with respect to increase in current density, indicating that the redox reaction is a diffusion controlled process, which might be rate limited by diffusion of electrolyte ions into the active materials.[54] The discharge curves initially show a drop in potential caused by internal resistance and are almost symmetric to their charge counterparts in the applied potential window, confirming that these PEDOT electrodes have promise as supercapacitor electrodes. The galvanostatic charge/discharge curves of other PEDOT electrodes for various charge/discharge current densities of 1, 2.5, 5, 7.5, 10, 12.5, 15, 17.5 and 20 A g^{-1} are shown in Fig. S8.† Variations of specific capacitance values with respect to different discharge current density of PEDOT electrodes are shown in Fig. 7(c). As expected, the 2.5 MR $FeCl_3$-based PEDOT nanodendrites exhibited higher specific capacitance value for all the tested discharge current densities because of optimum doping level and higher conjugation length of the polymer matrix. The specific capacitance values obtained from the charge/discharge test are in good agreement with those calculated using CV analysis. Moreover, at low discharge current density 1.25 and 2.5 MR $FeCl_3$-polymerized PEDOT nanoparticles exhibited similar specific capacitance values. This is mainly because of the existence of similar nanostructures of PEDOT allowing more electrolyte diffusion during redox reactions at low current density when compared with the other

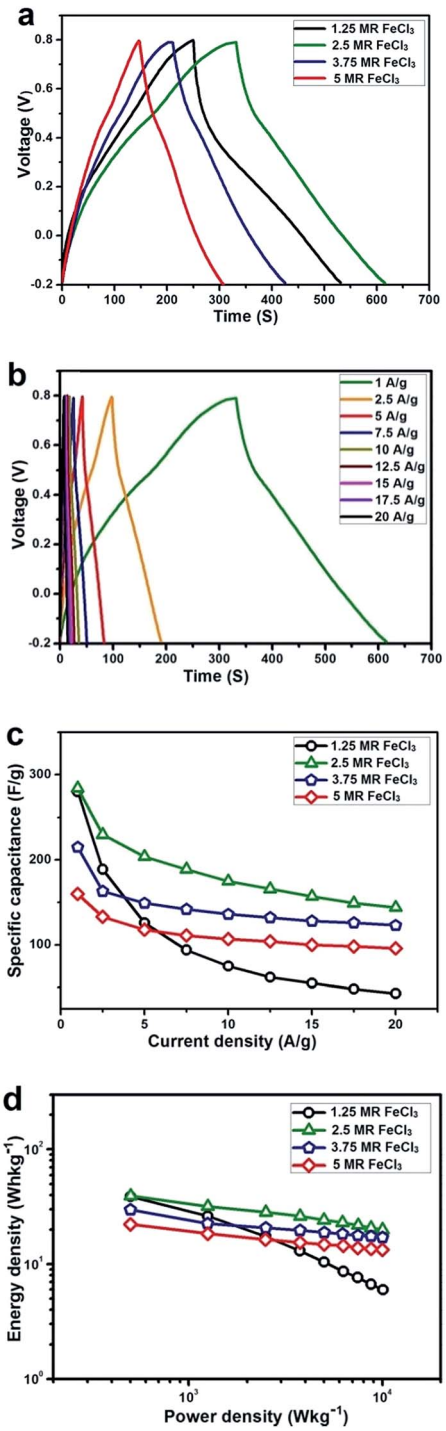

Fig. 7 (a) Galvanostatic charge discharge curves of the PEDOT electrodes at 1 A g^{-1} current density; (b) galvanostatic charge discharge curves of 2.5 MR $FeCl_3$-based PEDOT electrodes at different current densities (1 to 20 A g^{-1}); (c) variation of specific capacitance values with respect to different current density from 1 to 20 A g^{-1} of PEDOT electrodes and (d) Ragone plot of different MR of $FeCl_3$ synthesised PEDOT electrodes.

nanostructures. But, at higher discharge current densities the 1.25 MR $FeCl_3$-based PEDOT sample shows a drastic decline in specific capacitance value because of less involvement of the partially polymerized sample in the redox reaction process.

Fig. 7(d) shows the Ragone plots (energy density *vs.* power density) of the PEDOT electrodes. The energy density of 2.5 MR $FeCl_3$-based PEDOT electrodes increases from 20 W h kg^{-1} to 39.44 W h kg^{-1}, while the power density decreases from 10.08 kW kg^{-1} to 0.5 kW kg^{-1}. At the same time, the 1.25 MR $FeCl_3$ shows comparable energy density with highly diminished rate capability (38.88 W h kg^{-1} to 5.90 W h kg^{-1}) with almost the same power density (10.03 kW kg^{-1} to 0.5 kW kg^{-1}). Similarly, higher MR of $FeCl_3$-polymerized PEDOT electrodes show low and reasonable energy densities (29.86 W h kg^{-1} to 17.08 W h kg^{-1}) for 3.75 MR and (22.22 W h kg^{-1} to 13.33 W h kg^{-1}) for 5 MR of $FeCl_3$-based PEDOT electrodes. Therefore, the 2.5 MR $FeCl_3$-polymerization-based nanodendrite PEDOT electrode shows higher electrochemical capacitor performance than the other PEDOT electrodes.

The specific capacitance value of the present work and those of previous reports based on PEDOT electrodes are comparatively displayed in Fig. 8. In general, a high surface area with high conductivity of ECPs nanostructures are inclination towards superior supercapacitive performance. Therefore, optimization of proper controlled morphology and crystalline properties of ECPs to achieve metal-like high electrical properties was accomplished by simple thermal treatments or vapour phase polymerization synthesis. A hydrothermal method relies on the chemical reactions and change of reactants in a sealed heated aqueous solution, which lead to formation of highly conductive nanostructures. The PEDOT electrodes in this study exhibit higher specific capacitance values than those in previous reports, validating the possibility of employing these electrodes in electrochemical supercapacitors.

3.3.3 Electrochemical impedance spectroscopy. Electrochemical impedance spectroscopy (EIS) is an effective and reliable technique for acquiring clear information on electrochemical and charge transfer properties of supercapacitor electrode materials. The obtained Nyquist plots for PEDOT electrodes are shown in Fig. 9(a), with the inset showing a magnified image of the high-frequency region of the plot. The plots display a resistor part at the high-frequency region because of the diffusion effect of electrolyte and capacitor

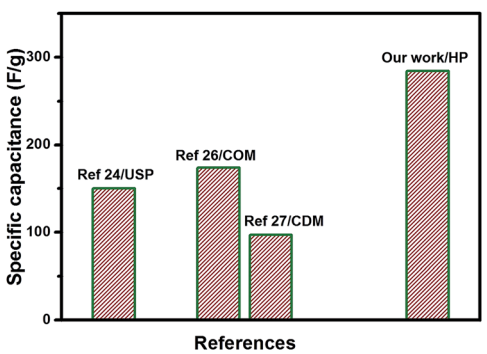

Fig. 8 Comparison of specific capacitance values of various PEDOT supercapacitor electrodes synthesized using $FeCl_3$ oxidant *via* different synthetic methods. (CDM – chemical deposition method; USP – ultrasonic spray polymerization; COM – chemical oxidative method and HP – hydrothermal polymerization.)

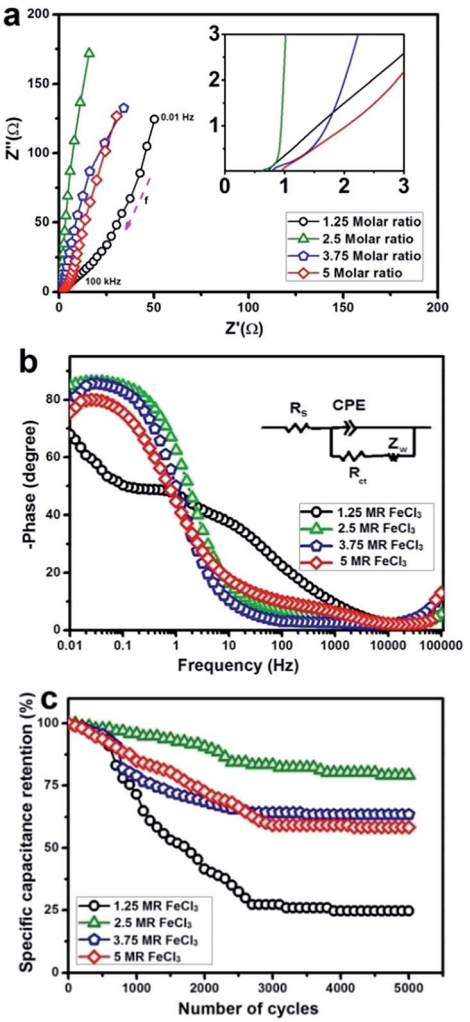

Fig. 9 (a) Nyquist plots; (b) Bode plots of PEDOT electrodes obtained from different MR of $FeCl_3$; (inset of (b) shows the equivalent circuit of fit) and (c) cycling stability of various nanostructured PEDOT electrodes tested for 5000 cycles at 10 A g^{-1} constant charge/discharge current density.

behaviour in the low-frequency region.[55,56] The high-frequency region intercept of the real axis Z' indicates the bulk solution resistance (internal resistance), which is a combination of ionic resistance of the electrolyte, the intrinsic resistance of the electroactive material and contact resistance at the interface of electroactive material and current collector.[57] The obtained Nyquist plots were modeled using the equivalent circuit shown in the inset of Fig. 9(b) using Zview software. The component R_s is the solution resistance of the cell, R_{ct} is the charge transfer resistance, CPE is the constant phase element and Z_w is the Warburg diffusion resistance. The EIS fitted parameters of various electrodes are listed in Table 1. The bulk solution resistance R_s values for different nanostructured PEDOT electrodes were found to be ~0.76, 0.70, 1 and 1.2 Ω for 1.25, 2.5, 3.75 and 5 MR $FeCl_3$-based PEDOT electrodes. It is clearly expressed that the 2.5 MR $FeCl_3$-polymerized nanodendrite PEDOT electrode exhibits a lower solution resistance than other MR of $FeCl_3$-based PEDOT electrodes. This is mainly because the higher conjugation length of the polymer chain of the polymer, with better conductivity and small particle size, can form more adhesion with the current collector than other samples. The charge transfer resistance R_{ct} is associated with the electron transfer process and, if the R_{ct} value is lower, it signifies the feasibility of the electron transfer process and, furthermore, the possibility of high pseudocapacitance for the electroactive materials.[58] The charge transfer resistance R_{ct} values were 0.77, 0.1, 3.8 and 5.5 Ω for 1.25, 2.5, 3.75 and 5 MR $FeCl_3$-polymerized PEDOT electrodes, respectively. These results reveal that 2.5 MR $FeCl_3$-polymerized nanodendrite PEDOT electrodes possess lower charge transfer resistance to attain more interfacial electron transfer process and diffusion of electroactive materials.

The Bode plots of PEDOT electrodes obtained from different MR of $FeCl_3$ are shown in Fig. 9(b). At lower frequencies, the phase angle approaches −90°, indicating that the supercapacitor electrodes almost behave like an ideal capacitor.[59,60] The Bode phase angle plot suggests that the 2.5 MR $FeCl_3$-polymerized PEDOT nanodendrite electrodes possess high capacitive behaviour with phase angle ~−85° among other PEDOT samples with −68°, −79° and −76° for 1.25, 3.75 and 5 MR $FeCl_3$-polymerized PEDOT nanoparticles, respectively.[56,61]

3.3.4 Cycling stability test. The long-term stability of conducting polymers is an important factor for their commercial applications as effective supercapacitor electrodes. The cycling stability retention of various MR $FeCl_3$-polymerized PEDOT electrodes was tested at 10 A g^{-1} constant current density for 5000 charge/discharge sequential cycles (Fig. 9(c)). The cycling stability plot depicts that the 2.5 MR $FeCl_3$-polymerized PEDOT nanodendrite electrode shows good cycling stability with ~79% retention of initial specific capacitance values after 5000 cycles. In comparison, specific capacitance retention was ~25, 64 and 59% for 1.25, 3.75 and 5 MR $FeCl_3$-based PEDOT electrodes, respectively, after 5000 cycles. The 1.25 MR $FeCl_3$-based PEDOT electrode shows much less retention stability compared with the other MR-based PEDOT electrodes, further confirming the insufficient oxidant during the polymerization process. The optimum doping level and higher conjugation length of polymer chain with high surface area and comparable crystallinity of the 2.5 MR $FeCl_3$-polymerized PEDOT nanodendrite structure-based electrodes makes it easier for ions accessing the polymer matrix and allowing store of higher charge. Overall electrochemical performance reveals that 2.5 MR $FeCl_3$-polymerized PEDOT nanodendrites are more promising

Table 1 Fitted EIS parameters of different molar ratios of $FeCl_3$-polymerized PEDOT electrodes

Molar ratio of $FeCl_3$	R_s/Ω	R_{ct}/Ω	Capacitance/F
1.25	0.76	0.77	0.044
2.5	0.70	0.10	0.091
3.75	1.0	3.80	0.087
5	1.2	5.0	0.067

supercapacitive electrode than other MR $FeCl_3$-polymerized PEDOT nanostructures.

4. Conclusion

In summary, PEDOT nanodendrites and nanospheres were synthesized *via* a facile, green and template-free hydrothermal polymerization process. This method provides a scalable process for synthesis of highly conducting and crystalline PEDOT nanomaterial. Nanodendrite morphologies were successfully controlled by choice of oxidant molar ratio in the precursor solutions. It was found that the different types of PEDOT nanoparticles have individual key properties of redox behaviours, electrochemical performance, cycling stability and ion diffusion. These PEDOT nanodendrites are potentially useful as supercapacitor electrode with binder-free form by determining their specific capacitance of 284 F g^{-1} with high energy density of 39.44 W h kg^{-1} and excellent cycling stability, which are among the highest yet reported. Thus, the simple hydrothermal polymerization method is an amenable route for synthesis of PEDOT nanodendrites as prospective supercapacitor electrode material for high energy storage devices.

Acknowledgements

The authors would like to acknowledge the authorities of Dongguk University-Seoul for their moral and financial support. The first author (M. R) acknowledges the Study and Research at Dongguk University (SRD) fellowship for the PhD Program.

References

1 P. Simon and Y. Gogotsi, *Nat. Mater.*, 2008, **7**, 845–854.
2 A. Rudge, J. Davey, I. Raistrick, S. Gottesfeld and J. P. Ferraris, *J. Power Sources*, 1994, **47**, 89–107.
3 S. Kirchmeyer and K. Reuter, *J. Mater. Chem.*, 2005, **15**, 2077–2088.
4 S. Ghosh, H. Remita, L. Ramos, A. Dazzi, A. Deniset-Besseau, P. Beaunier, F. Goubard, P. H. Aubert, F. Brisset and S. Remita, *New J. Chem.*, 2014, **38**, 1106–1115.
5 R. Xiao, S. I. Cho, R. Liu and S. B. Lee, *J. Am. Chem. Soc.*, 2007, **129**, 4483–4489.
6 B. H. Jones, K. Y. Cheng, R. J. Holmes and T. P. Lodge, *Macromolecules*, 2012, **45**, 599–601.
7 X. Bai, X. Hu, S. Zhou, J. Yan, C. Sun, P. Chen and L. Li, *Electrochim. Acta*, 2013, **106**, 219–225.
8 J. W. Kim and K. D. Suh, *J. Ind. Eng. Chem.*, 2008, **14**, 1–9.
9 T. L. Kelly, Y. Yamada, S. P. Y. Che, K. Yano and M. O. Wolf, *Adv. Mater.*, 2008, **20**, 2616–2621.
10 M. G. Han and S. H. Foulger, *Chem. Commun.*, 2004, 2154–2155, DOI: 10.1039/b409396h.
11 X. Zhang, J. S. Lee, G. S. Lee, D. K. Cha, M. J. Kim, D. J. Yang and S. K. Manohar, *Macromolecules*, 2006, **39**, 470–472.
12 J. Jang, M. Chang and H. Yoon, *Adv. Mater.*, 2005, **17**, 1616–1620.
13 J. Wu, Y. Li and W. Feng, *Synth. Met.*, 2007, **157**, 1013–1018.
14 B. H. Kim, D. H. Park, J. Joo, S. G. Yu and S. H. Lee, *Synth. Met.*, 2005, **150**, 279–284.
15 S. Patra and N. Munichandraiah, *J. Appl. Polym. Sci.*, 2007, **106**, 1160–1171.
16 J. Y. Kim, M. H. Kwon, Y. K. Min, S. Kwon and D. W. Ihm, *Adv. Mater.*, 2007, **19**, 3501–3506.
17 B. Winther-Jensen and K. West, *Macromolecules*, 2004, **37**, 4538–4543.
18 J. P. Lock, S. G. Im and K. K. Gleason, *Macromolecules*, 2006, **39**, 5326–5329.
19 S. G. Im and K. K. Gleason, *Macromolecules*, 2007, **40**, 6552–6556.
20 H. Chelawat, S. Vaddiraju and K. Gleason, *Chem. Mater.*, 2010, **22**, 2864–2868.
21 B. Winther-Jensen, J. Chen, K. West and G. Wallace, *Macromolecules*, 2004, **37**, 5930–5935.
22 P. Subramanian, N. Clark, B. Winther-Jensen, D. MacFarlane and L. Spiccia, *Aust. J. Chem.*, 2009, **62**, 133–139.
23 J. M. D'Arcy, M. F. El-Kady, P. P. Khine, L. Zhang, S. H. Lee, N. R. Davis, D. S. Liu, M. T. Yeung, S. Y. Kim, C. L. Turner, A. T. Lech, P. T. Hammond and R. B. Kaner, *ACS Nano*, 2014, **8**, 1500–1510.
24 Y. Zhang and K. S. Suslick, *Chem. Mater.*, 2015, **27**, 7559–7563.
25 A. J. Heeger, *Rev. Mod. Phys.*, 2001, **73**, 681–700.
26 Q. Zhao, R. Jamal, L. Zhang, M. Wang and T. Abdiryim, *Nanoscale Res. Lett.*, 2014, **9**, 557.
27 J. S. Sohn, U. M. Patil, S. Kang, S. Kang and S. C. Jun, *RSC Adv.*, 2015, **5**, 107864–107871.
28 Q. Yang, Z. Lu, J. Liu, X. Lei, Z. Chang, L. Luo and X. Sun, *Prog. Nat. Sci.: Mater. Int.*, 2013, **23**, 351–366.
29 A. Elschner, *PEDOT principles and applications of an intrinsically conductive polymer*, CRC Press, Boca Raton, FL, 2011.
30 M. Fabretto, K. Zuber, C. Hall, P. Murphy and H. J. Griesser, *J. Mater. Chem.*, 2009, **19**, 7871–7878.
31 H. Ding, M. Wan and Y. Wei, *Adv. Mater.*, 2007, **19**, 465–469.
32 S. J. T. Rezaei, Y. Bide and M. R. Nabid, *Synth. Met.*, 2011, **161**, 1414–1419.
33 N. Kim, B. H. Lee, D. Choi, G. Kim, H. Kim, J. R. Kim, J. Lee, Y. H. Kahng and K. Lee, *Phys. Rev. Lett.*, 2012, **109**, 106405.
34 A. Lenz, H. Kariis, A. Pohl, P. Persson and L. Ojamäe, *Chem. Phys.*, 2011, **384**, 44–51.
35 K. E. Aasmundtveit, E. J. Samuelsen, L. A. A. Pettersson, O. Inganäs, T. Johansson and R. Feidenhans'l, *Synth. Met.*, 1999, **101**, 561–564.
36 C. Jiang, G. Chen and X. Wang, *Synth. Met.*, 2012, **162**, 1968–1971.
37 J. W. Choi, M. G. Han, S. Y. Kim, S. G. Oh and S. S. Im, *Synth. Met.*, 2004, **141**, 293–299.
38 K. E. Aasmundtveit, E. J. Samuelsen, O. Inganäs, L. A. A. Pettersson, T. Johansson and S. Ferrer, *Synth. Met.*, 2000, **113**, 93–97.
39 N. Kim, S. Kee, S. H. Lee, B. H. Lee, Y. H. Kahng, Y. R. Jo, B. J. Kim and K. Lee, *Adv. Mater.*, 2014, **26**, 2268–2272.
40 B. Winther-Jensen, M. Forsyth, K. West, J. W. Andreasen, P. Bayley, S. Pas and D. R. MacFarlane, *Polymer*, 2008, **49**, 481–487.

41 W. W. Chiu, J. Travaš-Sejdić, R. P. Cooney and G. A. Bowmaker, *J. Raman Spectrosc.*, 2006, **37**, 1354–1361.
42 M. Łapkowski and A. Proń, *Synth. Met.*, 2000, **110**, 79–83.
43 S. Garreau, G. Louarn, J. P. Buisson, G. Froyer and S. Lefrant, *Macromolecules*, 1999, **32**, 6807–6812.
44 F. Wei, L. Yu, W. Jun, N. Hideki, F. Akihiko, O. Masanori and Y. Katsumi, *J. Phys.: Condens. Matter*, 2007, **19**, 186220.
45 S. Geetha and D. C. Trivedi, *Synth. Met.*, 2005, **155**, 232–239.
46 D. Wu, J. Zhang, W. Dong, H. Chen, X. Huang, B. Sun and L. Chen, *Synth. Met.*, 2013, **176**, 86–91.
47 T. W. Kim, H. Y. Woo, W. G. Jung, D. W. Ihm and J. Y. Kim, *Thin Solid Films*, 2009, **517**, 4147–4151.
48 L. Groenendaal, F. Jonas, D. Freitag, H. Pielartzik and J. R. Reynolds, *Adv. Mater.*, 2000, **12**, 481–494.
49 H. Seok Jang, C. Justin Raj, W. G. Lee, B. Chul Kim and K. Hyun Yu, *RSC Adv.*, 2016, **6**, 75376–75383.
50 M. A. Ali, H. H. Kim, C. Y. Lee, H. S. Soh and J. G. Lee, *Met. Mater. Int.*, 2009, **15**, 977–981.
51 C. Jin, F. Yang and W. Yang, *J. Appl. Polym. Sci.*, 2006, **101**, 2518–2522.
52 J. Yang and S. Gunasekaran, *Carbon*, 2013, **51**, 36–44.
53 D. P. Dubal, S. V. Patil, A. D. Jagadale and C. D. Lokhande, *J. Alloys Compd.*, 2011, **509**, 8183–8188.
54 F. Wolfart, D. P. Dubal, M. Vidotti, R. Holze and P. Gómez-Romero, *J. Solid State Electrochem.*, 2016, **20**, 901–910.
55 C. Lei, N. Amini, F. Markoulidis, P. Wilson, S. Tennison and C. Lekakou, *J. Mater. Chem. A*, 2013, **1**, 6037–6042.
56 H. Mi, X. Zhang, X. Ye and S. Yang, *J. Power Sources*, 2008, **176**, 403–409.
57 M. H. Yeh, C. P. Lee, C. Y. Chou, L. Y. Lin, H. Y. Wei, C. W. Chu, R. Vittal and K. C. Ho, *Electrochim. Acta*, 2011, **57**, 277–284.
58 R. Ramya, R. Sivasubramanian and M. V. Sangaranarayanan, *Electrochim. Acta*, 2013, **101**, 109–129.
59 A. Lewandowski, A. Olejniczak, M. Galinski and I. Stepniak, *J. Power Sources*, 2010, **195**, 5814–5819.
60 P. L. Taberna, P. Simon and J. F. Fauvarque, *J. Electrochem. Soc.*, 2003, **150**, A292–A300.
61 D. Antiohos, G. Folkes, P. Sherrell, S. Ashraf, G. G. Wallace, P. Aitchison, A. T. Harris, J. Chen and A. I. Minett, *J. Mater. Chem.*, 2011, **21**, 15987–15994.